Applied Physics Express 12, 037001 (2019)
https://doi.org/10.7567/1882-0786/ab0397

LETTER

Low-frequency noise spectroscopy of charge-density-wave phase transitions in vertical quasi-2D 1T-TaS_2 devices

Ruben Salgado[1], Amirmahdi Mohammadzadeh[1], Fariborz Kargar[1], Adane Geremew[1], Chun-Yu Huang[1], Matthew A. Bloodgood[2], Sergey Rumyantsev[1,3], Tina T. Salguero[2], and Alexander A. Balandin[1*]

[1]*Nano-Device Laboratory (NDL) and Phonon Optimized Engineered Materials (POEM) Center, Department of Electrical and Computer Engineering, University of California, Riverside, CA 92521 United States of America*
[2]*Department of Chemistry, University of Georgia, Athens, GA 30602 United States of America*
[3]*Center for Terahertz Research and Applications, Institute of High Pressure Physics, Polish Academy of Sciences, Warsaw 01-142 Poland*

[*]E-mail: balandin@ece.ucr.edu

Received January 6, 2019; revised January 25, 2019; accepted January 31, 2019; published online February 15, 2019

We report results regarding the electron transport in *vertical* quasi-two-dimensional (2D) layered 1T-TaS_2 charge-density-wave (CDW) devices. The low-frequency noise spectroscopy was used as a tool to study changes in the *cross-plane* electrical characteristics of the quasi-2D material below room temperature. The noise spectral density revealed strong peaks—changing by more than an order-of-magnitude—at the temperatures closely matching the electrical resistance steps. Some of the noise peaks appeared below the temperature of the commensurate to nearly-commensurate CDW transition, possibly indicating the presence of the debated *hidden* phase transitions. These results confirm the potential of the noise spectroscopy for investigations of electron transport and phase transitions in novel materials. © 2019 The Japan Society of Applied Physics

The charge-density-wave (CDW) phase is a macroscopic quantum state consisting of a periodic modulation of the electronic charge-density accompanied by a periodic distortion of the atomic lattice in metallic crystals.[1–3] Recently, the field of CDW materials and devices experienced a true renaissance.[4–15] The renewed interest has been driven by layer-control of CDW materials, such as quasi-two-dimensional (2D) crystals of 1T-TaS_2 and other transition metal dichalcogenides (TMDs). Unlike classical bulk CDW materials with the quasi-1D crystalline structure, certain members of the layered TMD family exhibit unusually high transition temperatures to various CDW phases, opening up the possibility of practical applications for CDW devices.[13–17] The 2D crystal structure of TMDs allows one to exfoliate or grow layers with few-nanometer thicknesses, creating conditions for greater control of the CDW phase transitions with temperature or electric field, as well as enabling integration with other 2D materials.[13–17]

One of the most interesting quasi-2D CDW TMD materials is 1T-TaS_2. At $T = 545$ K, it undergoes a transition from the normal metallic phase to the incommensurate (IC) CDW phase; at $T = 355$ K, it transforms to the nearly commensurate (NC) CDW phase; and finally, in the temperature range from $T = 150$ to 180 K, it changes to the commensurate (C) CDW phase.[4,7–9,12] The NC-CDW phase consists of C-CDW domains separated by regions of IC-CDW phase. The high transition temperature of the IC to NC CDW phase, along with the possibility of controlling this transition with voltage, permits the practical implementation of such materials. Some of us recently demonstrated the 1T-TaS_2 voltage-controlled oscillator based on the current switching driven by voltage-tuned CDW phase transitions.[12] These 1T-TaS_2 CDW devices, operational at room temperature (RT), exhibit high radiation hardness,[14] and can be used for high frequency and information processing applications.[12,16,17]

Almost all prior studies of CDW phenomena and CDW-based devices in 1T-TaS_2 and other TMDs have focused on the electron transport along the quasi-2D planes of these materials.[4–18] We are aware of only one prior detailed report on *cross-plane* electronic transport in vertical 1T-TaS_2 devices.[19] The cross-plane transport is expected to have interesting features because, in some layered TMDs, the crystal lattice distortion during the CDW phase transition affects the cross-plane direction even more strongly than the in-plane direction.[11] The previous study of the cross-plane transport revealed step-like changes in electrical resistivity at temperatures between 50 K and 100 K,[19] which are substantially lower temperatures than those reported for the well-known transition between the C-CDW and NC-CDW transition.[4,7–9,12] These observations may be related to discussions about the possible existence and nature of metastable *hidden* states and phase transitions in 1T-TaS_2.[19–25] A range of possible scenarios, e.g. Mott transitions or interlayer re-ordering of the stacking structure, are under consideration. Furthermore, there are indications that the hidden states can be particularly interesting in the vertical CDW devices.[19]

Investigation of electron transport in the *vertical* quasi-2D 1T-TaS_2 CDW devices is more challenging than that in "conventional" planar CDW devices. The stress due to the mismatch of the temperature coefficients of the materials can affect the transport characteristics of the vertical devices more strongly than those of planar devices. In addition, it is often difficult to identify possible phase transitions in the relatively small changes in the current–voltage (I–V) characteristics. These considerations provide strong motivation for developing new experimental methods and approaches applicable to investigating cross-plane transport in layered CDW materials. Recently, we demonstrated that low-frequency noise (LFN) measurements can be used for identification of the transition between the NC to IC CDW phases and CDW sliding in a "conventional" planar 1T-TaS_2 device.[13] In this Letter, we show that LFN spectroscopy is effective for studying the electron transport and CDW transitions in the vertical 1T-TaS_2 devices, and in fact, this method can identify the CDW and potential hidden state transitions with higher accuracy than using the I–V characteristics.

High-quality 1T-TaS_2 crystals were prepared by the chemical vapor transport (CVT) method, from the elements using I_2 as the transport agent, via quenching from the crystal growth temperature. The details of this synthesis and corresponding material characterization data have been reported by some of us elsewhere.[11,12,26] The vertical

CDW devices (see Fig. 1 for schematic) were fabricated via mechanical exfoliation from CVT-grown crystals and an all-dry transfer method. The device fabrication process can be described briefly in the following steps. First, the bottom electrodes were patterned by the electron beam lithography (EBL; LEO Supra) on a SiO_2/Si substrate. Immediately after, the layers of Ti/Au metal were deposited by electron beam evaporation (EBE; Temescal BJD). The thin 1T-TaS_2 layers were exfoliated from bulk crystals onto an ultra-clean PDMS-glass stamp, which was mounted onto a home-built transfer stage.[12–14,29] The stage was equipped with a micromanipulator to align and transfer the exfoliated layers from the PDMS surface onto the bottom electrode. The thin layers of exfoliated hexagonal boron nitride (*h*-BN) were then placed overlapping the edge of 1T-TaS_2 layers using the same dry-stamp transfer technique in order to avoid any unwanted edge contacts. Finally, the top electrodes made of Ti and Au metals were fabricated using EBL and EBE.

The optical image of a typical 1T-TaS_2 vertical CDW device used in this study is shown in the inset to Fig. 2(a). The cross-sectional area and thickness of the 1T-TaS_2 layer in these devices were around 0.5 μm^2 and 90 nm, respectively. The temperature dependent current–voltage (I–V) characteristics of the devices were measured in a cryogenic probe station (Lakeshore TTPX) with a semiconductor analyzer (Agilent B1500). The devices were cooled down to 78 K at a ramp up rate of 1.5 K min^{-1} and heated at the same rate back to RT. The tested devices reached temperature stability between the heating and cooling cycle while their resistance was measured at a DC bias sweep from 0 to 10 mV. In Fig. 2(a) we present the measured resistance of a representative two-terminal vertical 1T-TaS_2 device as a function of temperature. The resistance hysteresis associated with the commensurate (C) to NC CDW phases can be observed at the transition temperature, T_C, which is in the range reported in previous studies.[4,7–9,12] During the measurements we observed changes in the resistance at temperatures below T_C. To investigate these changes, more 1T-TaS_2 vertical devices with similar structure and dimensions were fabricated and tested. Figure 2(b) shows the temperature dependent resistance of three different vertical devices measured below the C-CDW–NC-CDW phase transition temperature. The measurements were performed in the cooling cycle. The resistance drop can be seen in all three measured devices, in the temperature range from 80 to 100 K, which is substantially below the C-CDW–NC-CDW phase transition temperature.

The noise spectra of the signals amplified by the low-noise amplifier (Stanford Research 560) were measured with a dynamic signal analyzer (Stanford Research 560). The devices under test were DC biased with a "quiet" battery-potentiometer circuit in order to minimize the 60 Hz noise and its harmonics from the electrical grid. The noise measurements were conducted in the two-terminal device configuration. Because the contact resistance was negligibly small compared to the 1T-TaS_2 layer resistance, the measured noise response was dominated by the CDW material of interest. The short-circuit current fluctuations were calculated following the conventional formula $S_I = S_V\,[(R_L + R_D)/(R_L R_D)]^2$, where S_I is the current noise spectral density, S_V is the voltage noise spectral density, R_L and R_D are the load and device resistances, respectively.

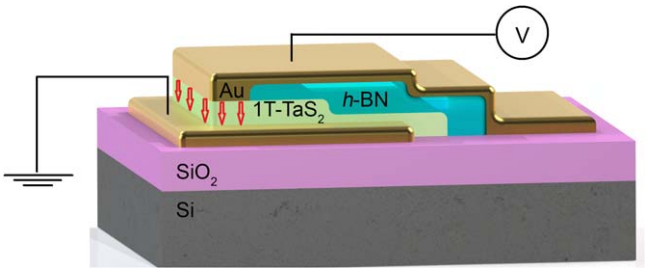

Fig. 1. (Color online) Schematic of the vertical quasi-2D 1T-TaS_2 charge-density-wave device. The electrical current flows perpendicular to the atomic planes of 1T-TaS_2 layered crystal. The direction of the current is shown with the red arrows.

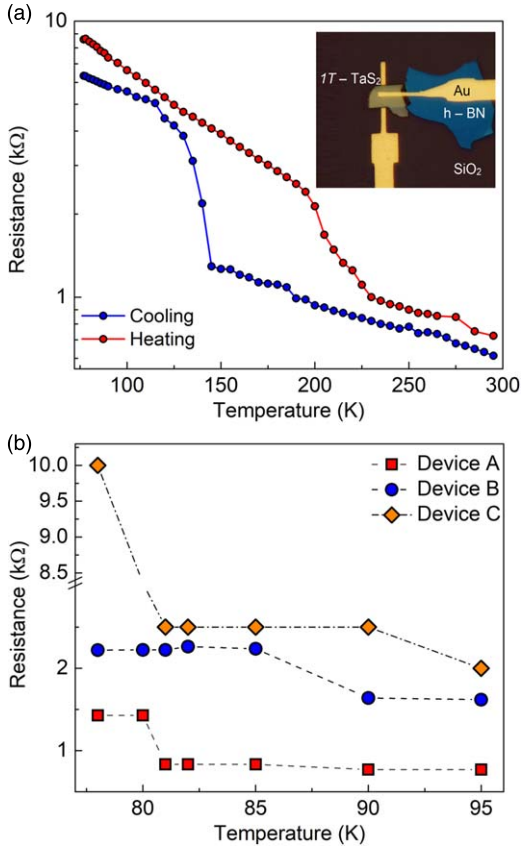

Fig. 2. (Color online) (a) Electrical resistance of a representative vertical 1T-TaS_2 device measured in the cooling and heating cycles over a wide range of temperature. The insert shows an annotated optical microscopy image of the vertical device. (b) Electrical resistance of three different vertical 1T-TaS_2 devices measured below the well-known commensurate to nearly-commensurate charge-density-wave transition temperature. Note that all devices show steps in the resistance in the temperature range from 80 to 100 K.

Details of our low noise measurement procedures can be found elsewhere.[13,29,30]

Figure 3(a) shows the voltage noise spectral density, S_V, as a function of frequency for a representative vertical 1T-TaS_2 device under DC bias voltage, V_B, varying from 0.6 to 80 mV. The data were taken at RT. All spectra follow the $S_V \propto 1/f$ behavior without any signatures of generation–recombination (G–R) bulges. In Fig. 3(b) we present the current noise spectral density, S_I, as a function of the current though the device, which demonstrates perfect scaling with I^2. This proportionality implies that current does not drive the fluctuations but merely accentuates their visibility following Ohm's law.[31] It also

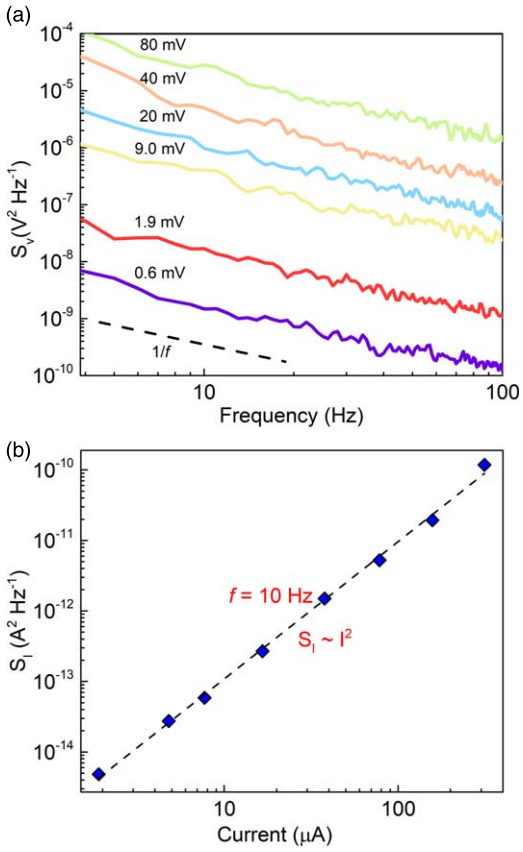

Fig. 3. (Color online) (a) Low-frequency voltage referred noise spectral density as a function of frequency for a vertical 1T-TaS_2 charge-density-wave device. The room-temperature data are shown for the bias voltage ranging from 0.6 to 80 mV. Note that all noise spectra are of the 1/*f* type without any signatures of the Lorentzian bulges. (b) Noise spectral density as a function of the electric current between two device terminals at a fixed frequency $f = 10$ Hz.

suggests the absence of electromigration, strong self-heating or other damage to the device as a result of passing the current.

We performed the low-temperature electrical resistance and LFN measurements on the vertical 1T-TaS_2 device as it was heated from 77 K to above the C-CDW–NC CDW phase transition temperature, T_C. In Fig. 4, we present the measured electrical resistance and the normalized current noise spectral density, S_I/I^2, as a function of temperature. The noise data were accumulated at $V_B = 13$ mV and frequency of 10 Hz. The sudden drop in the resistance observed around 160 K is associated with the well-established C-CDW–NC-CDW phase transition. As one can see, the noise spectral density reveals a peak around the same temperature. The noise peak is clearly associated with this phase transition, in line with prior observation for the in-plane CDW devices.[13] The drop in resistance around $T = 100$ K, observed in several vertical 1T-TaS_2 devices, is substantially below the C-CDW–NC-CDW phase transition temperature, and also is accompanied by the peak in the noise spectral density.

It is interesting to note that the noise spectra measured at temperatures away from the phase transition temperature are always of the 1/*f* type (see also Ref. 13). The noise spectra within the noise peak, which corresponds to the phase transition, have the form of the well-defined Lorentzian. Figure 5 shows an example of the noise spectra at temperature $T = 98$ K, which corresponds to the hidden phase transition, in the vertical configuration devices studied here.

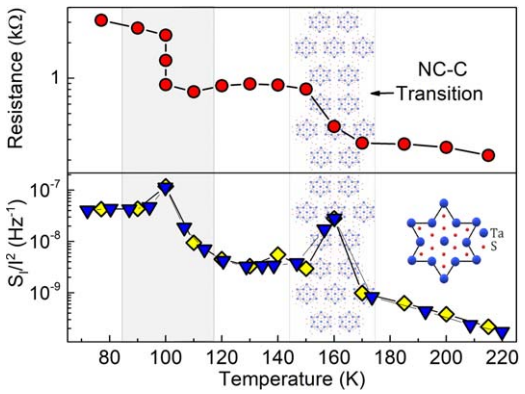

Fig. 4. (Color online) Electrical resistance (upper panel) and normalized current noise spectral density (lower panel) as the functions of temperature. The noise data were measured at the bias of $V_{SD} = 13$ mV and frequency $f = 10$ Hz. The decrease in resistance at $T_C = 160$ K corresponds to the well-known commensurate to nearly-commensurate CDW transition. A diagram, depicting the reconstruction of 13 Ta atoms into hexagonal clusters, is shown to illustrate the phase transition. A distinctive noise peak is observed at the same temperature T_C. Below the C-CDW–NC-CDW phase transition temperature one can see another step in the resistance with the corresponding peak in the noise spectral density. The noise data are shown for two experimental runs to ensure reproducibility.

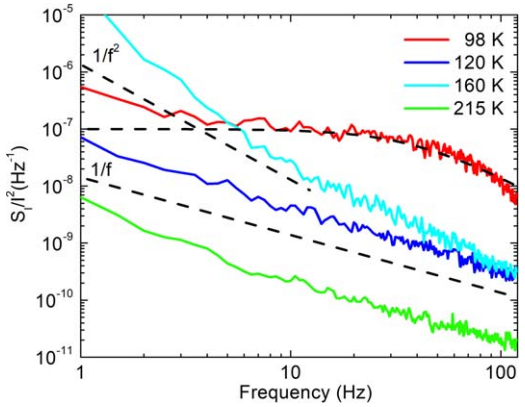

Fig. 5. (Color online) Normalized low-frequency current noise spectral density as a function of frequency. The data are presented for four different temperatures. The 1/*f* and $1/f^2$ spectra are shown with the dashed lines for comparison. Note the Lorentzian peak in the noise spectrum taken near the temperature $T = 98$ K. The spectrum taken near $T = 160$ K has the peak below 1 Hz.

At $f > 8$ Hz, the noise spectrum at $T = 98$ K is close to the Lorentzian shape shown by the dashed curve, expressed as $S_I/I^2 \sim A/[1 + (2\pi f\tau)^2]$, where A is the constant and $\tau = 4 \times 10^{-3}$ s is the time constant, which characterizes the dynamic of the phase transition. The characteristic time τ of the Lorentzian spectra depends on the specifics of the transition and applied voltage. The noise spectrum at $T = 160$ K, which corresponds to the C–NC CDW phase transition, reveals the characteristic Lorentzian frequency well below 1 Hz, and only the tail of the $1/f^2$ part of the spectrum is observed. It is important to note that the noise spectra measured at the same temperature but in "conventional" lateral CDW devices do not show signs of the Lorentzian shape. This fact suggests that the Lorentzian-type spectra exhibited in the vertical configuration is not a result of the G–R process but rather correspond to the phase transition.

A sharp increase of noise near and at the phase transition is known for other materials.[31–35] It can be associated with abrupt changes in the resistance and instability of the characteristics of the material at the phase transition. We have previously observed two pronounced maxima in the noise spectra of in-plane 1T-TaS_2 devices at the bias voltages, which were exactly corresponding to the onset of CDW sliding and the NC-to-IC phase transition.[13] Lorentzian peaks are often observed in the LFN spectra. This type of the noise spectra is associated with random processes, which are characterized by the well-defined time constant. The most common example is the G–R noise in semiconductors, which appears due to the fluctuations of a local level occupancy. The physics of Lorentzian peaks in CDW materials is more complicated and still not completely understood.[13]

In conclusion, we have described the cross-plane electron transport in vertical quasi-2D layered 1T-TaS_2 CDW devices using LFN spectroscopy to study changes in the electrical characteristics below RT. We observed two steps in electrical resistivity in the temperature range from 150 to 180 K, and in the range from 80 to 100 K. The normalized LFN spectral density revealed strong peaks at these transition points, changing by more than an order-of-magnitude. The higher temperature feature was associated with the well-known transition between the C-CDW and NC-CDW states. The lower temperature transition may indicate the presence of the "hidden" CDW phase. These results further support the potential of the LFN spectroscopy for investigating electron transport in vertically-stacked quasi-2D materials.

Acknowledgments The work at UCR and UGA was supported, in part, by the National Science Foundation (NSF) Emerging Frontiers of Research Initiative (EFRI) 2-DARE project: Novel Switching Phenomena in Atomic MX_2 Heterostructures for Multifunctional Applications (NSF EFRI-1433395). A.A.B. also acknowledges the UC—National Laboratory Collaborative Research and Training Program—University of California Research Initiatives (LFR-17-477237). S. R. also acknowledges partial support from the Center for Terahertz Research and Applications (CENTERA) in the framework of the International Research Agenda program of the Foundation for Polish Science co-financed by the European Union under the European Regional Development Fund. Nanofabrication was performed in the Center for Nanoscale Science and Engineering (CNSE) Nanofabrication Facility at UC Riverside.

ORCID iDs Ruben Salgado https://orcid.org/0000-0002-4869-7607 Fariborz Kargar https://orcid.org/0000-0003-2192-2023 Alexander A. Balandin https://orcid.org/0000-0002-9944-7894

1) G. Grüner, Rev. Mod. Phys. **60**, 1129 (1988).
2) S. V. Zaitsev-Zotov, Phys. Usp. **47**, 533 (2004).
3) R. E. Thorne, Phys. Today **49**, 42 (1996).
4) B. Sipos, A. F. Kusmartseva, A. Akrap, H. Berger, L. Forró, and E. Tutiš, Nat. Mater. **7**, 960 (2008).
5) K. Rossnagel, J. Phys.: Condens. Matter **23**, 213001 (2011).
6) P. Goli, J. Khan, D. Wickramaratne, R. K. Lake, and A. A. Balandin, Nano Lett. **12**, 5941 (2012).
7) L. Stojchevska, I. Vaskivskyi, T. Mertelj, P. Kusar, D. Svetin, S. Brazovskii, and D. Mihailovic, Science **344**, 177 (2014).
8) Y. Yu et al., Nat. Nanotechnol. **10**, 270 (2015).
9) M. Yoshida, Y. Zhang, J. Ye, R. Suzuki, Y. Imai, S. Kimura, A. Fujiwara, and Y. Iwasa, Sci. Rep. **4**, 7302 (2014).
10) M. Porer, U. Leierseder, J.-M. Ménard, H. Dachraoui, L. Mouchliadis, I. E. Perakis, U. Heinzmann, J. Demsar, K. Rossnagel, and R. Huber, Nat. Mater. **13**, 857 (2014).
11) R. Samnakay, D. Wickramaratne, T. R. Pope, R. K. Lake, T. T. Salguero, and A. A. Balandin, Nano Lett. **15**, 2965 (2015).
12) G. Liu, B. Debnath, T. R. Pope, T. T. Salguero, R. K. Lake, and A. A. Balandin, Nat. Nanotechnol. **11**, 845 (2016).
13) G. Liu, S. Rumyantsev, M. A. Bloodgood, T. T. Salguero, and A. A. Balandin, Nano Lett. **18**, 3630 (2018).
14) G. Liu, E. X. Zhang, C. D. Liang, M. A. Bloodgood, T. T. Salguero, D. M. Fleetwood, and A. A. Balandin, IEEE Electron Device Lett. **38**, 1724 (2017).
15) K. Takase, S. Hiramoto, T. Fukushima, K. Sato, C. Moriyoshi, and Y. Kuroiwa, Appl. Phys. Express **10**, 123001 (2017).
16) A. G. Khitun, G. Liu, and A. A. Balandin, IEEE Trans. Nanotechnol. **16**, 860 (2017).
17) A. G. Khitun, A. K. Geremew, and A. A. Balandin, IEEE Electron Device Lett. **39**, 1449 (2018).
18) D. Svetin, I. Vaskivskyi, P. Sutar, E. Goreshnik, J. Gospodaric, T. Mertelj, and D. Mihailovic, Appl. Phys. Express **7**, 103201 (2014).
19) D. Svetin, I. Vaskivskyi, S. Brazovskii, and D. Mihailovic, Sci. Rep. **7**, 46048 (2017).
20) Y. Tokura, J. Phys. Soc. Jpn. **75**, 011001 (2006).
21) H. Ichikawa, Nat. Mater. **10**, 101 (2011).
22) J. C. Petersen et al., Phys. Rev. Lett. **107**, 177402 (2011).
23) I. Vaskivskyi, I. A. Mihailovic, S. Brazovskii, J. Gospodaric, T. Mertelj, D. Svetin, P. Sutar, and D. Mihailovic, Nat. Commun. **7**, 11442 (2016).
24) L. Ma et al., Nat. Commun. **7**, 10956 (2016).
25) A. W. Tsen et al., Proc. Natl Acad. Sci. **112**, 15054 (2015).
26) J. Renteria et al., J. Appl. Phys. **115**, 34305 (2014).
27) Z. Yan, G. Liu, J. M. Khan, and A. A. Balandin, Nat. Commun. **3**, 827 (2012).
28) A. Geremew et al., IEEE Electron Device Lett. **39**, 735 (2018).
29) G. Liu, S. Rumyantsev, M. A. Bloodgood, T. T. Salguero, M. Shur, and A. A. Balandin, Nano Lett. **17**, 377 (2017).
30) A. K. Geremew, S. Rumyantsev, M. A. Bloodgood, T. T. Salguero, and A. A. Balandin, Nanoscale **10**, 19749 (2018).
31) A. A. Balandin, *Noise and Fluctuation Control in Electronic Devices* (American Scientific, Los Angeles, 2002).
32) Z. Topalian, S.-Y. Li, G. A. Niklasson, C. G. Granqvist, and L. B. Kish, J. Appl. Phys. **117**, 25303 (2015).
33) M. Kawasaki, P. Chaudhari, and A. Gupta, Phys. Rev. Lett. **68**, 1065 (1992).
34) H. K. Kundu, S. Ray, K. Dolui, V. Bagwe, P. R. Choudhury, S. B. Krupanidhi, T. Das, P. Raychaudhuri, and A. Bid, Phys. Rev. Lett. **119**, 226802 (2017).
35) D. M. Fleetwood, IEEE Trans. Nucl. Sci. **62**, 1462 (2015).